Astron. Astrophys. 252, 835–841 (1991)

ASTRONOMY AND ASTROPHYSICS

General relativistic effects in astrophysical jets

D. Vokrouhlický and V. Karas

Department of Astronomy and Astrophysics, Charles University, Švédská 8, CS-150 00 Prague, Czechoslovakia

Received May 25, accepted August 23, 1991

Abstract. General relativistic effects in the dynamics of optically thin jets are studied. Jet particles move along the rotation axis of the central compact object (Kerr black hole) in the radiation field of an accretion disk (relativistic α-viscosity thin disk). Attention is paid mainly to the effects in the close vicinity of the central object: what is the influence of rotation of the black hole, gravitational and Doppler redshift, and the bending of photon paths on the radiation field along particle's trajectory and how this may affect the terminal Lorentz factor of the jet. Within the model adopted, we conclude that the most important general relativistic contribution comes only indirectly through the dependence of the local disk luminosity on the hole's rotation. These effects do not otherwise seem to affect the terminal speed of the jet significantly. Several typical particle trajectories outside of the rotation axis are constructed numerically.

Key words: galaxies: jets of – black holes – relativity – radiation mechanism: general

1. Introduction

The problem of the dynamics of test particles influenced by combined radiative and gravitational fields has an important astrophysical application in the theory of optically thin jets emanating from the cores of active galactic nuclei (AGN). In the early eighties it was realised that the radiation field may exert a significant Compton drag on a particle moving with a relativistic speed along the accretion disk funnel (Abramowicz & Piran, 1980; Sikora & Wilson, 1981). The dragging force determines an upper limit of the the jet speed and imposes in this way constraints on models of jet acceleration (Phinney, 1987). More recently, Melia & Königl (1989) studied the jet-radiation interaction with astrophysically relevant details carefully taken into account, but ignored the effects of the strong gravitational field near the central object. In particular, they verified that for a given radiation field (determined by the disk parameters), maximum terminal Lorentz factor of the jet γ_f is independent of its initial value γ_i near the black hole.

In this paper, we will study how general relativistic effects affect the velocity of the jet moving along the symmetry axis of an accretion disk. We adopt the scenario in which the activity of the AGN results from the interaction of a compact object (presumably a supermassive black hole) with a disk. We basically consider the bending of light rays from the disk near the black hole, redshift, and the influence of rotation of the central object. On the other hand, we employ a simple model of the jet-radiation interaction (described by the Thomson cross section), and ignore the effects of the magnetic field. The influence of recaptured photons on the disk structure is also ignored. Our approach has been strongly influenced by the work of Abramowicz et al. (1990) who studied an analogous problem with a spherically symmetric configuration. We assume an axially symmetric gravitational field (the Kerr metric). Relevant equations are summarized in the next Section. In the subsequent example, we consider the radiation field which acts on the electron-positron plasma ($m = m_{\text{electron}}$; naturally, ordinary plasma with $m = m_{\text{proton}}$ is much less sensitive to the radiation effects). Radiation is generated by a standard α-viscosity thin disk with relativistic corrections taken into account (Novikov & Thorne, 1973). [Thin accretion disks do not seem to be a viable source delivering fuel to AGN; Begelman et al. (1989), Shlosman et al. (1990). However, there are serious problems with geometrically thick flows and dense star clusters as well. The thin disk model is possibly an appropriate description of the innermost regions of AGN, which is where general relativistic effects become important.] The origin of the dragging force is, therefore, somewhat different than that considered by, e.g., Sikora & Wilson (1981), where an isotropic part of the radiation in the funnel was important.

We compare the values of γ_f in the case when general relativistic effects are considered with those when the corrections are ignored. Although the influence of separate effects is evident, we find that in total, with the disk local luminosity profile given, the standard approach (ignoring bending of light rays and redshift) is satisfactory. This result is gratifying in view of previous works on this subject, which ignored gravitation; on the other hand, such a conclusion only strengthens the suspicion that general relativistic effects in astrophysical jets can hardly be discovered directly by measuring speed of jets. What does influence the results is a dependence of the disk luminosity on angular momentum of the central object and boundary conditions near the inner edge of the disk. Unfortunately, present relativistic models of accretion disks are far from being established and generally accepted (for a review see, e.g., Abramowicz, 1987).

In the last Section we will construct several test particle trajectories integrated numerically outside of the axis of symmetry. The aim is to clarify whether pressure of the disk radiation, affected by strong gravitational field near the black hole, can contribute to collimation of jet particles to the symmetry axis.

Send offprint requests to: D. Vokrouhlický

2. Basic equations

We start with the general relativistic equation of motion of a test particle under the influence of the radiation field (see, e.g., Abramowicz et al., 1990)

$$v^\mu v^\nu{}_{;\mu} = \frac{\sigma}{m} h^\nu_\mu T^{\mu\lambda} v_\lambda, \tag{1}$$

where v^μ, σ and m denote particle's four-velocity, cross-section and mass, $h_{\mu\nu} = (g_{\mu\nu} - v_\mu v_\nu)$ is the projection tensor, $g_{\mu\nu}$ is the background metric, and $T^{\mu\lambda}$ is the stress-energy tensor of the radiation field. Here, we adopt geometric units with $c = G = 1$. Let us denote $n^{(i)}$ $(i = r, \theta, \phi)$ components of a unit vector in the direction of a photon from the radiation field in the local static spherical frame located at the position of the particle, $n^{(t)} = 1$. Tetrad components of the stress-energy tensor can be expressed in terms of the radiation field intensity $I_P(\theta, \phi)$ integrated over the local sky of the particle:

$$T^{(\mu)(\lambda)} = \int I_P n^{(\mu)} n^{(\lambda)} d\Omega. \tag{2}$$

Specifying the disk model, we can calculate $T^{(\mu)(\lambda)}$ numerically and then integrate Eq. (1) to obtain the speed of the jet as a function of distance from the central object. As we pay more attention to the relativistic effects within a simple model rather than to astrophysical details of the accretion disk structure, we describe the disk by a well-understood model of the α-viscosity disk (Sect. 5.9 of Novikov & Thorne, 1973).

From here on, we adopt a non-dimensional form of the Kerr metric in Boyer-Lindquist coordinates

$$ds^2 = (\Delta/\Sigma)(dt - a\sin^2\vartheta d\varphi)^2 \tag{3}$$

$$-(\sin^2\vartheta/\Sigma)[(x^2 + a^2)d\varphi - a dt]^2 - (\Sigma/\Delta)dx^2 - \Sigma d\vartheta^2,$$

$x = r/M$, $\Delta = x^2 - 2x + a^2$, $\Sigma = x^2 + a^2\cos^2\vartheta$, M mass of the central object, aM^2 its angular momentum.

In the case of motion along the symmetry axis, we denote β velocity of the particle (jet) measured in the local static frame, $\gamma = (1 - \beta^2)^{-1/2}$. Eq. (1) reduces to the form:

$$\frac{d\beta}{dx} = \frac{\Sigma}{\beta\gamma^2\Delta}\left\{\kappa\mu\gamma\left(\frac{\Delta}{\Sigma}\right)^{1/2}\left[(1+\beta^2)\mathscr{F} - \beta\mathscr{E}\right]\right.$$

$$\left. - \frac{x^2 - a^2\cos^2\vartheta}{\Sigma^2}\right\}, \tag{4}$$

with $\kappa = 2\sigma M_\odot/m$, $\mu = \dot{M}_{17} M_\odot/M$ ($\dot{M}_{17}$ accretion rate in units of 10^{17}g/s), and

$$\mathscr{F}(x) = \int_0^\pi F(x_{em})\,\mathscr{R}(x, x_{em})\,\mathscr{S}(x, x_{em})\sin\theta\cos\theta d\theta, \tag{5}$$

$$\mathscr{E}(x) = \int_0^\pi F(x_{em})\,\mathscr{R}(x, x_{em})\,\mathscr{S}(x, x_{em})\sin\theta(1 + \cos^2\theta)\,d\theta. \tag{6}$$

$F(x_{em})$ is the local energy flux in the direction perpendicular to the disk evaluated in the frame co-rotating with the disk matter at radius x_{em} (Novikov & Thorne, 1973; our μF corresponds to F in this reference). Two points—one with the radial coordinate x on the axis and the other with the radial coordinate x_{em} in the disk—are connected by a photon ray $\tilde{x}(\vartheta)$ in the Kerr metric:

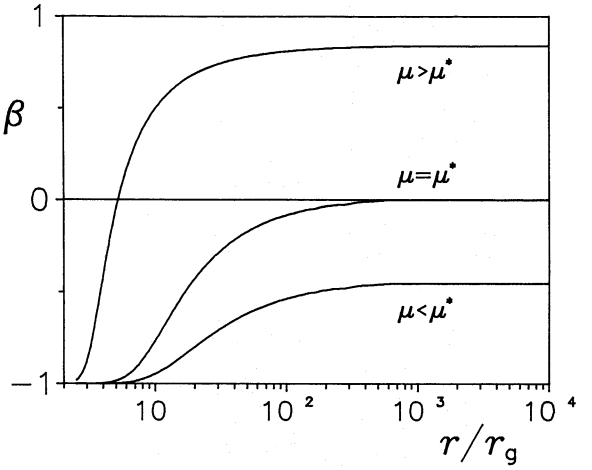

Fig. 1. Three typical saturation curves of the electron-positron plasma moving along the symmetry axis in the α-viscosity disk model

$$\frac{d\tilde{x}}{d\vartheta} = \frac{[\tilde{x}^4 + (a^2 - \eta)\tilde{x}^2 + 2\tilde{x}(\eta + a^2) - a^2\eta]^{1/2}}{(\eta + a^2\cos^2\vartheta)^{1/2}}, \tag{7a}$$

$$\frac{d\varphi}{d\vartheta} = \frac{2a\tilde{x}}{\Delta(\eta + a^2\cos^2\vartheta)^{1/2}}, \tag{7b}$$

$$\frac{dt}{d\vartheta} = \frac{(\tilde{x}^2 + a^2)^2 - \Delta a^2\sin^2\vartheta}{\Delta(\eta + a^2\cos^2\vartheta)^{1/2}}, \tag{7c}$$

$\tilde{x}(0) = x$, $\tilde{x}(\pi/2) = x_{em}$, $\eta(\theta, x) = \Delta^{-1}[x^4 + a^2x(x+2)]\sin^2\theta - a^2\cos^2\theta$ [x_{em} being a function of θ through the solution of Eq. (7) which is needed for the evaluation of the integrals (5)–(6)]. Along the photon ray with a four-momentum p^μ, the redshifted intensity $I/(p^\mu\eta_\mu)^4$ is conserved, where η_μ is the local observer's four-velocity. This leads to the redshift function $\mathscr{R}(x, x_{em})$ in (5)–(6), which transforms the radiation intensity in the frame co-rotating with the disk, I_{DCF}, to the local static frame on the axis:

$$\mathscr{R}(x, x_{em}) = \left[\frac{\Sigma^2}{\Delta^2}\right]_x \left[\frac{\Delta^4\mathscr{C}^2}{x^8(\mathscr{A}\mathscr{G} + 2ax^{-5/2}\mathscr{H})^4}\right]_{x_{em}}, \tag{8}$$

where $\mathscr{G} = 1 - 2x^{-1} + ax^{-3/2}$, $\mathscr{C} = 1 - 3x^{-1} + 2ax^{-3/2}$, $\mathscr{A} = 1 + a^2x^{-2} + 2ax^{-3}$, $\mathscr{H} = 1 - 2ax^{-3/2} + a^2x^{-2}$. Function $\mathscr{S}(x, x_{em})$ is the source function characterizing angular distribution of radiation in I_{DCF}. Unless stated otherwise, in the following examples we assume the distribution corresponding to electron scattering, $\mathscr{S} = \frac{3}{7}(1 + 2\cos\Theta)$ with Θ given by

$$\tan^2\Theta = \left[\frac{1}{\Delta}\left(\frac{dx}{d\vartheta}\right)^2 + \frac{\mathscr{B}^2\mathscr{D}}{\mathscr{C}}\left(\frac{d\varphi}{d\vartheta} - \Omega\frac{dt}{d\vartheta}\right)^2\right]_{x_{em}}, \tag{9}$$

where $\Omega = x^{-3/2}\mathscr{B}^{-1}$, $\mathscr{B} = 1 + ax^{-3/2}$, $\mathscr{D} = 1 - 2x^{-1} + a^2x^{-2}$. [Electron scattering is a prevailing mechanism in the inner regions of the α-viscosity disk, where most of the radiation is generated. For derivation of functions $\mathscr{R}(x, x_{em})$, $\mathscr{S}(x, x_{em})$, see Appendix.]

Although the disk is described by the three parameters—viscosity parameter (α), mass of the central object (M), and accretion rate ($\dot{M}_{17}$)—discussed dynamics of test particles depends only on the parameter μ, which has been closely related to the accretion rate by Abramowicz et al. (1988). In their paper, the

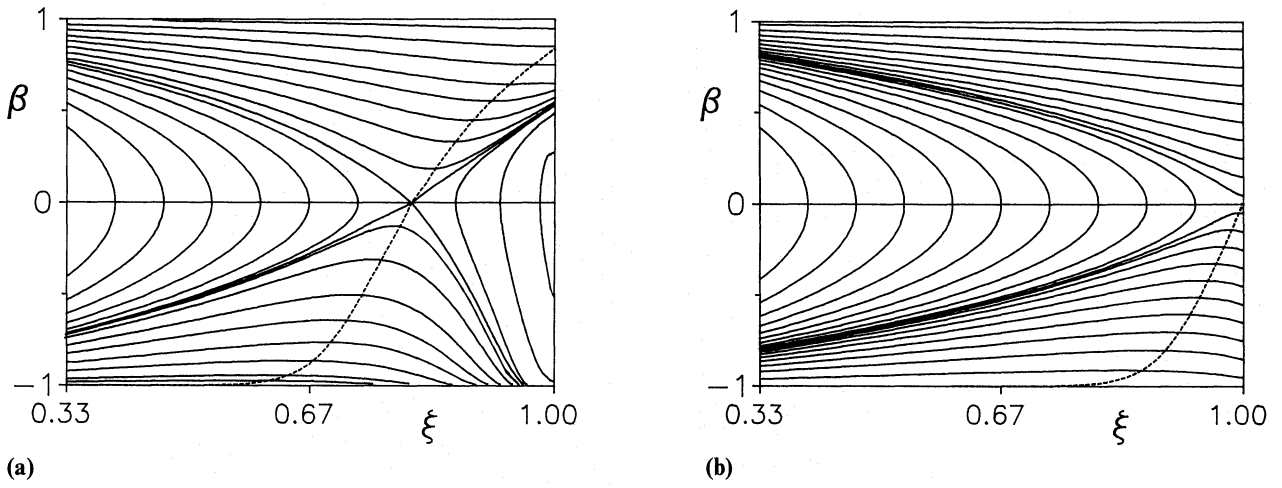

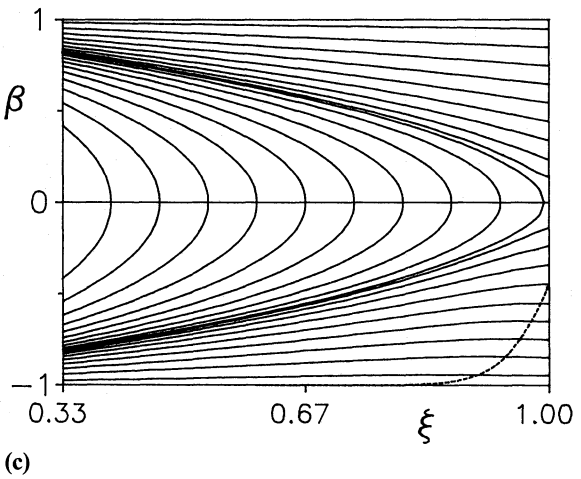

Fig. 2. Structure of the solutions $\beta(\xi)$ of the equation of motion (4) for the three cases: (a) $\mu > \mu^*$, (b) $\mu = \mu^*$, and (c) $\mu < \mu^*$. The *solid* curves show the particle trajectories satisfying Eq. (10). The *dashed* ones draw the saturation curves in corresponding cases (see the text)

fact that the Shakura-Sunyaev α-disk models cannot be continued (due to thermal instability) above some critical value of μ is discussed in greater detail (see also Szuszkiewicz, 1990). In agreement with Abramowicz et al. (1988) we accept $\mu \cong 0.1$ for this limiting value, although it was derived using quasi-Newtonian gravitational potential of Paczyński & Wiita (1980) for static systems. A corresponding result for the relativistic modification of the α-disk models (qualitative or quantitative) probably has not been mentioned in the literature as yet. Abramowicz et al. (1988) also described a more luminous branch of the α-disks (slim disks). With significantly higher luminosity, slim disks are capable of accelerating ordinary plasma. In this paper, we restrict ourselves to standard α-disks, but the approach can be easily applied to models with modified luminosity profiles.

In the case when the particle motion is not restricted to the axis of symmetry, Eq. (1) in its general form is needed. Analogous concepts—the photon ray bending in the background geometry and propagation of the radiative intensity along this ray as described by the redshift function $\mathscr{R}(x, x_{\rm em})$ and the source function $\mathscr{S}(x, x_{\rm em})$ [Eqs. (8)–(9)]—can be taken into consideration. It is straightforward to write down all the relevant expressions explicitely.

3. Motion along the axis of symmetry

In this Section, we study the motion of the jet particles along the symmetry axis of the disk, $\vartheta = 0, \pi$. First, we discuss the configuration with a non-rotating black hole; next, rotation of the black hole is included (rotation axis parallel with the axis of the disk).

3.1. Schwarzschild background metric

We can rewrite Eq. (4) in the form

$$\frac{d\beta}{d\xi} = \frac{1}{2\xi\beta\gamma^2}\left\{\frac{4\kappa\mu\gamma\xi^{1/2}}{(1-\xi)^2}\left[(1+\beta^2)\mathscr{F} - \beta\mathscr{E}\right] - 1\right\}, \tag{10}$$

where $\xi(x) = 1 - 2x^{-1}$; in this case, Eqs. (8)–(9) yield $\mathscr{R}(x, x_{\rm em}) = (1 - 3x_{\rm em}^{-1})^2\xi^{-2}$, $\cos\Theta = (x/x_{\rm em})[\xi(x_{\rm em})/\xi(x)]^{1/2}$ $[1 - 1/(x_{\rm em}\xi(x_{\rm em}))]^{1/2}\sin\theta$.

Figure 1 shows saturation curves of the solution of Eq. (10) defined by $d\beta/d\xi = 0$. Analogous curves have been constructed in previous models with gravitational effects ignored (e.g., Sikora & Wilson, 1981). Saturation curve (as introduced by Abramowicz et al., 1990) is an appropriate tool for qualitative investigation of the test particle acceleration or deceleration. We find that for $\mu \equiv \mu^* \cong 0.00605$ the saturation curve approaches 0 at infinity ($\xi \to 1$), which means that the gravitational attraction on a particle at rest is just balanced by the radiative repulsion. In this sense, μ^* describes disks with luminosity which affects the particles analogously to the Eddington luminosity of spherical objects. For $\mu > \mu^*$ saturation curves intersect the $\beta = 0$ axis in a critical point of Eq. (4).

Figure 2 shows $\beta(\xi)$ solutions of Eq. (10) for the three values of μ from Fig. 1. For $\mu < \mu^*$ particles are only slightly affected by the radiation and the whole portrait reminds the free fall case: $\gamma\xi^{1/2} = const$. For $\mu > \mu^*$ saturation velocity changes its sign. Near the central object ($\xi = 1/3$ corresponds to a photon orbit $x = 3$) gravitational effects dominate again, but at large distances the curves are modified significantly. The critical point is of the

saddle type, in contrast to the case of a spherically symmetric source of Abramowicz et al. (1990).

Particles ejected from the vicinity of the central object with a great speed with respect to the local static frame ($\gamma_i \gg 1$, definite value should follow from a given scenario of the jet pre-acceleration) "see" blue-shifted radiation in the direction of their motion. Two effects contribute to the shift: special relativistic Doppler effect and gravitational shift of the radiation coming from more distant regions of the disk. Besides, light rays are bent by gravity. Thus one could expect more efficient deceleration when relativistic effects connected with the motion of photons are taken into account. However, these effects are cancelled by relativistic corrections to the disk model, which become important mainly in the inner region, where most of the radiation of the disk is generated. The difference is demonstrated mathematically through the $\mathscr{L}$-function in the radiative flux (Novikov & Thorne, 1973, for a complete derivation of its form see Page & Thorne, 1974). Graphs of resulting terminal Lorentz factors are shown in Fig. 3: for a given disk model and initial Lorentz factor γ_i at $r = r_i$ value of the terminal factor γ_f is nearly insensitive to the relativistic corrections, except for the innermost values of r_i. One can also observe (Fig. 3) that the curves γ_f as a function of the initial radius r_i are only very slightly affected by the value of γ_i close to the central object, in accordance with the results of Melia & Königl (1989) on maximum terminal values of γ_f (cf. Fig. 4 of this reference).

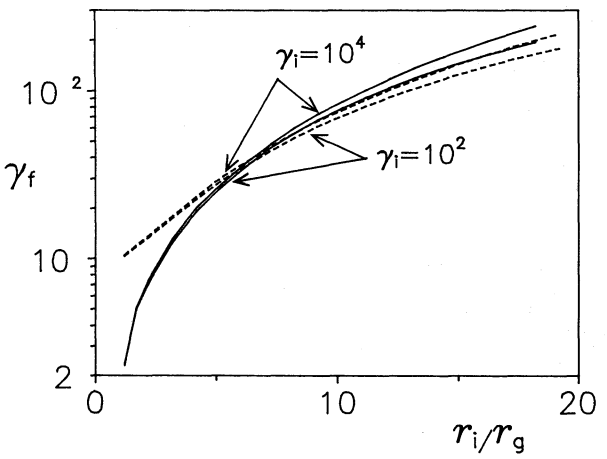

Fig. 3. Terminal Lorentz factor of the jet γ_f is shown as a function of initial radial coordinate r_i. Corresponding values of the initial Lorentz factor γ_i near the disk are given with the curves. Solid lines are solutions of complete Eq. (4) with all relativistic effects taken into account; dotted lines correspond to the case when Doppler and gravitational redshifts and relativistic correction in the $\mathscr{L}$-function of the disk structure are ignored [Shakura-Sunyaev (1973) model] and photon paths are straight lines

Figure 4 shows γ_f as a function of the accretion rate parameter μ. For γ_i large enough, $\log(\gamma_f)$ is inversely proportional to $\log(\mu)$. This follows immediately from the fact that for various μ solutions of Eq. (4) in the limit when radiative terms dominate can be related to each other through a function of $\xi : \gamma_\mu(\xi)\mu = \omega(\xi)$ (say). In other words, when the "gravitational" term $(x^2 - a^2\cos^2\vartheta)/\Sigma^2$ in Eq. (4) is ignored, the equation of motion analogous to Eq. (10) of Melia & Königl (1989) is obtained. In the case of non-relativistic particles or less radiative disks, gravitation of the central object starts to play a dynamical

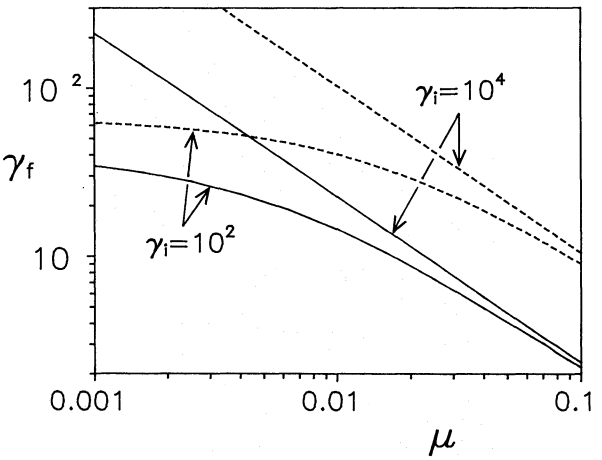

Fig. 4. Terminal Lorentz factor of the jet γ_f is shown as a function of the accretion rate parameter μ; here, values of γ_i are shown with the curves, $r_i = 1.2r_g$ for definiteness. Solid and dotted lines as in Fig. 3

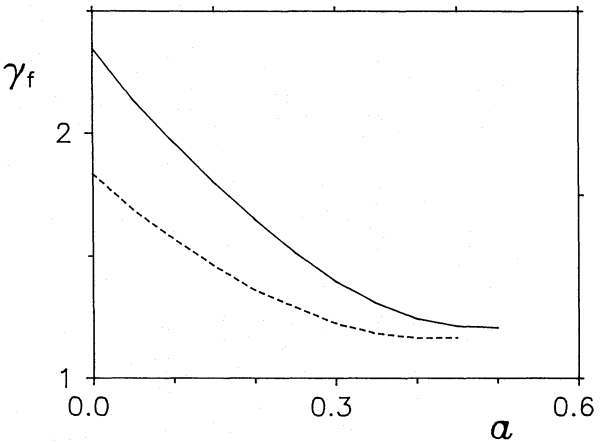

Fig. 5. Graph γ_f is shown as a function of the rotation parameter a in the Kerr background metric; $r_i = 1.2\,M$, $\gamma_i = 10^4$, $\mu = 0.1$. The solid line has been computed with the electron scattering source function (see the text). For comparison, the dotted line corresponds to the isotropic distribution of radiation in the disk co-rotating frame, $\mathscr{S} = 1$. Because luminosity of innermost regions of the disk increases with a and the deceleration of the jet thus becomes more efficient, one can find a critical value of the rotation parameter, above which jet particles with given initial conditions do not reach distant regions where γ_f is determined (here, $r_f = 5\ 10^4\,M$)

role, in addition to the Compton drag. This can be observed in Fig. 4. For weakly radiating disks, $\mu \ll 1$, the γ_f curves saturate to the value $\gamma_i\xi_i^{1/2}$ which corresponds to the purely gravitational limit with all the effects of the radiation field ignored. Naturally, in this region the value of γ_f is not influenced by the photon dynamics and both newtonian and relativistic solutions converge to nearly the same value (up to the difference of the order 1). On the other hand, the upper limit to γ_f is given by the maximum terminal Lorentz factors, as discussed by Melia & Königl (1989).

3.2. Kerr background metric

Compared to the non-rotating case, marginally stable orbits of particles co-rotating with the hole are located at lower radii when the central black hole rotates. Thus, co-rotating disks can extend

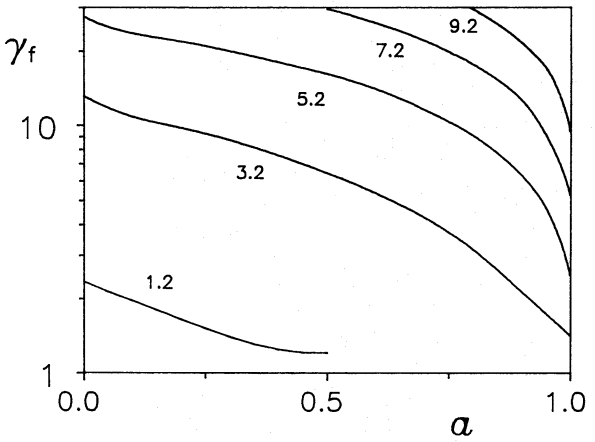

Fig. 6. Graphs of γ_f as in Fig. 5 but for various values of r_i/M given with the curves (see the text)

nearly to the horizon. Besides, the accretion rate given, it can be seen (Thorne, 1974) that inner regions of the disk near a rotating compact object are significantly more luminous (by the factor of about 350 for a 'canonically' rotating Kerr black hole with $a = 0.9982$) than in the non-rotating case. As the most luminous regions are located near the inner edge of the disk, Compton drag force on a particle increases rapidly with angular momentum of the central black hole. [Luminosity of the disk also increases with the accretion rate. However, the dependence on μ is only linear in the range considered and the a-dependence is thus more profound (Novikov & Thorne, 1973).]

There is no obvious way to identify configurations with different values of angular momentum of the central object (or with various disk models). One can compare results obtained with configurations with the same accretion parameter μ, eliminating the explicit dependence of the disk structure on the rotation of the central object. (Here, a is just a parameter by which different configurations are labeled.) One can also identify configurations with the same total luminosity. In this latter case, systems with different a need rescaling of μ according to (Thorne, 1974)

$$\mu_{\text{new}} = \frac{1 - E^{\dagger}(a_{\text{old}})}{1 - E^{\dagger}(a_{\text{new}})}\mu_{\text{old}}, \tag{11}$$

where $E^{\dagger}(a)$ is the energy of the marginally stable circular geodesic in the equatorial plane. Certainly, one can search for a different 'identification rule'. We accept the first concept, as stated above.

The general character of the solutions of Eq. (4) from Sect. 3.1 (Figs. 1–4) remains unchanged by the rotation of the black hole. For example, in the case of a canonically rotating black hole the value of the accretion parameter μ^* for which the saturation curve approaches 0 at infinity is $\mu^*_{|a=0.9982} \cong 0.00283$, in contrast to $\mu^*_{|a=0} \cong 0.00605$ in the Schwarzschild case. Let us formulate this result from the more physical point of view : chosen $\mu = \mu^*_{|a=0.9982}$ for the value of the accretion rate parameter and zero velocity as an initial condition for the test particle located at infinity on the symmetry axis, or simply at infinity in the Schwarzschild case, we maintain that

(i) if $a = 0.9982$ the particle would stay at rest,
(ii) if $a = 0$ the particle would begin to fall towards the hole (see the corresponding particle trace in Fig. 2c).

The behaviour of the gravity term in Eq. (4) is the same in both cases, but the radiative flux $\mathscr{F}$ given by Eq. (5) is greater in case (i). This fact is partially obscured due to the complexity of Eq. (5). However, the total luminosity of the disk (Thorne, 1974)

$$\left(dE/dt\right)_{\text{rad,tot}} \cong \mu\left(1 - E^{\dagger}(a)\right)\left(M/M_{\odot}\right) \tag{12}$$

is a closely related quantity. Keeping μ and M fixed, the disk around the rotating hole has greater luminosity compared to the non-rotating case due to the binding energy of the innermost disk orbit being greater (the orbit is situated nearer to the hole). The same is true for the radiative flux $\mathscr{F}$. Analogously, with $\mu = 0.1$, the terminal Lorentz factor corresponding to the saturation curve of the electron-positron plasma is $\gamma_{f,a=0.9982} \cong 2.15$, while $\gamma_{f,a=0} \cong 1.72$. The physical basis for this result is exactly the same as in the previous example. The rapidly rotating disks radiate more energy. Their radiation is generated mainly in the inner region, which is much more compact in comparison to the non-rotating case. However, we can conclude that these results are of the same order of magnitude although local disk luminosity does depend on a significantly. The saddle type of the critical point remains unchanged as well.

On the other hand, values of γ_f for a particle with definite initial conditions r_i, γ_i may depend on a significantly as shown in Fig. 6. The strong decrease of the terminal Lorentz factor in this numerical experiment might seem to contradict the previous results. One has to realize that the discussion in the previous paragraph deals with *the infinite region*, while this experiment depends mainly on processes in *the region near the hole*. Sharp fall of the initial Lorentz factor of the particle, γ_i, occurs predominantly in the vicinity of the hole. Due to this fact, higher luminosity of the rotating configurations leads to greater efficiency of deceleration. Naturally, the results depend strongly on the method of identifying the disks around black holes with different a as mentioned above. In Figs. 5–6 we accepted a constant value of μ. If we considered disks with equal total luminosity we would obtain γ_f nearly independent on parameter a because scaling formula [Eq. (11)] compensates the decrease in γ_f which is evident in Fig. 6. But as the rotating disk is closer to the point-like source of radiation, we would get slightly smaller deceleration efficiency of the rotating configuration when compared to systems with the same total luminosity. This argument results in a slightly greater terminal Lorentz factor when rotating black holes are considered and disks with equal luminosities are compared.

4. Test particle trajectories

Acceleration and collimation of a particle under radiation pressure of a thick disk has been studied by, e.g., Sikora & Wilson (1981). In their paper, zero-mass limit was adopted and gravity was ignored. On the other hand, possible effects of gravitational pre-collimation of jet particles to the axis of symmetry in the Kerr space-time have been studied by Bičák et al. (1991) with only moderate results (when $a^2 \leqq 1$).

Analogously, within a thin disk model a significant collimation due to the disk radiation cannot be expected if additional electrodynamic or magnetohydrodynamic effects are not considered. Nevertheless, we have constructed several test particle trajectories near the Schwarzschild black hole with radiation effects of the disk included (Fig. 7). Electron-positron plasma is assumed and two sets of the trajectories [given by Eq. (1)] starting

just above the disk surface are shown: Those starting at rest with respect to the local frame co-rotating with the disk surface (solid lines), and those starting at rest with respect to static observers (dashed lines). Question which arises within this context is, wheter radiative pressure of photons coming from the disk, bended and blue-shifted by the black hole's gravity can contribute to collimation. As can be seen in Fig. 7, only the particles with trajectories which start near the inner edge of the disk could be collimated by the radiative effects in this approach. In the Kerr backround metric, considering the results of Bičák et al. (1991) and the fact that the maximum of the local disk luminosity is located closer to the black hole than in the Schwarzschild case, one should not expect significantly more efficient collimation when both effects of rotation of a black hole and radiation of a thin disk were taken into account.

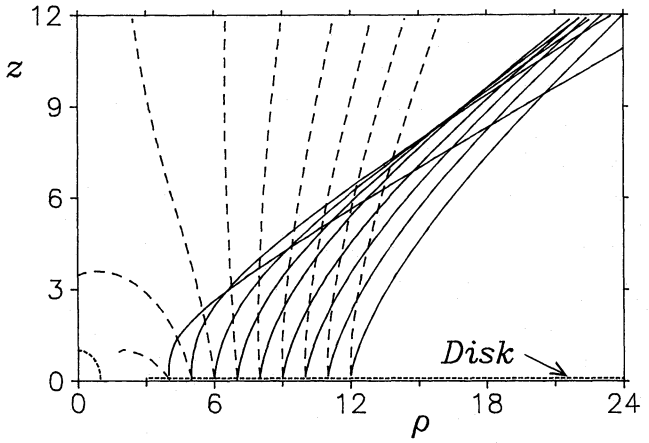

Fig. 7. The projection of the trajectories of test particles with $m = m_e$, $\sigma = \sigma_T$ under the influence of the disk radiation and the gravity of a spherical central object; $\rho = r\sin\vartheta$, $z = r\cos\vartheta$. Two sets of the test particles are drawn : *solid* curves for initially co-rotating with the disk particles, *dashed* curves for those initially at rest with respect to the distant observers. In both cases the particles start from the surface of the disk

5. Conclusions

In this paper, stimulated by the work of Abramowicz et al. (1990) we studied general relativistic effects within a simple model of the jet. In particular we plotted the terminal Lorentz factor of the jet particles as a function of the accretion rate parameter and initial conditions near the black hole. Rather strong dependence on the initial location of the particle could seem to contradict to the results of the quoted paper. It should be pointed out that we employ the disk model with the Eddington parameter intrinsically much smaller unity. In fact, this is the thin disk assumption. In the low Eddington regime Abramowicz et al. (1990) do not detect any common value of the terminal Lorentz factor for all the initial conditions in particular agreement with our results.

At present, our results do not seem to be very encouraging to those who wish to detect the general relativistic effects in AGN by study speed of jets. However, an important contribution of these effects may enter into considerations by affecting the accretion disk structure (which is a question to be solved). Moreover, there is no straightforward rule to identify disks around black holes with different angular momentum parameters. On the other hand, adopting an appropriate disk model, we can confirm analogous results of previous papers on this subject (cf. Melia & Königl, 1989) in which general relativistic effects were ignored. This result is not self-evident in advance because redshift factor and bending of light affect the radiation of the disk near the hole significantly.

With the thin disk model adopted, we could not find any significant contribution to pre-collimation of the jet due to (gravitationally affected) radiation pressure.

Acknowledgements. The authors are grateful to Drs. M. Abramowicz, A. Königl and A. Lanza for valuable comments. This work was supported in part by the IBM Academic Initiative in Czechoslovakia.

Appendix

Here, we derive the form of the redshift function, $\mathscr{R}(x, x_{em})$, and the source function, $\mathscr{S}(x, x_{em})$, from Sect. 2. We define two local reference frames:

(i) $\mathscr{I}_1$ is the local frame of a static observer located on the symmetry axis at the position of the particle, $r = xM$. Four-velocity of its origin expressed in Boyer-Lindquist coordinates is $\eta_1^\mu = (\Sigma^{1/2}\Delta^{-1/2}, 0, 0, 0)$.

(ii) $\mathscr{I}_2$ is the local frame of an observer co-rotating with the disk at the equatorial plane with radial coordinate $r_{em} = x_{em}M$. Four-velocity of its origin is $\eta_2^\mu = \eta_2^t(1, 0, 0, \Omega)$, $\eta_2^t = x^2\Delta^{-1}\mathscr{C}^{-1/2}(\mathscr{A}\mathscr{G} + 2ax^{-5/2}\mathscr{H})_{|x_{em}}$.

The origins of both frames are connected by a photon ray [Eq. (7)]. The intensity conservation law reads $I/(p^\mu\eta_\mu)^4 = const$. Because the photon crosses the symmetry axis, $p_\phi = 0$. Stationarity of the model yields $p_t = const$. Thus, intensity I_P measured in the frame $\mathscr{I}_1$ is related to I_{DCF} in $\mathscr{I}_2$ by the relation

$$I_P = I_{DCF}\mathscr{R}(x, x_{em}),$$

which from one point of view is the definition of our redshift function $\mathscr{R}(x, x_{em})$ and simultaneously yields the expression given in Eq. (8).

Now, we derive the formula for the source function $\mathscr{S}(x, x_{em})$ in the case of scattering due to electrons. Distribution of the radiation intensity in the frame $\mathscr{I}_2$ can be approximated by the function $\mathscr{S} = \frac{3}{7}(1+2\cos\Theta)$ (Thorne, 1974; our $\mathscr{S}$ corresponds to πS in this reference). Here, Θ denotes the angle between normal to the disk surface and the direction of the photon as measured in $\mathscr{I}_2$:

$$\tan^2\Theta = \frac{(p^{(r)})^2 + (p^{(\varphi)})^2}{(p^{(\vartheta)})^2},$$

where $p^{(r)}, p^{(\vartheta)}, p^{(\varphi)}$ are components of the photon four-momentum with respect to local tetrad $\mathbf{e}_\mu^{(a)}$ of the frame $\mathscr{I}_2$. As the observer in the frame $\mathscr{I}_2$ measures zero velocity of the disc particles at his location, one obtains $\mathbf{e}_t^{(\varphi)} = -\mathbf{e}_\varphi^{(\varphi)}\Omega$, where $\Omega = d\varphi/dt$ stands for the relativistic Keplerian velocity of the particles on circular geodesics in the disc plane. Substituting the explicit form of the rest frame $\mathbf{e}_\mu^{(a)}$ (see Novikov & Thorne, 1973) to the expression for $\tan\Theta$, we obtain Eq. (9).

References

Abramowicz M.A., 1987, in: General Relativity and Gravitation, ed. M.A.H. MacCallum, Cambridge University Press, Cambridge, p. 1
Abramowicz M.A., Piran T., 1980, ApJ 241, L7
Abramowicz M.A., Czerny B., Lasota J.P., Szuszkiewicz E., 1988, ApJ 332, 646
Abramowicz M.A., Ellis G.F.R., Lanza A., 1990, ApJ 361, 470
Begelman M.C., Frank J., Shlosman I., 1989, in: Theory of Accretion Disks, eds. F. Meyer, W. Duschl, J. Frank, E. Meyer-Hofmeister, Kluwer, Dordrecht
Bičák J., Semerák O., Hadrava P., 1991, in preparation
Melia F., Königl A., 1989, ApJ 340, 162
Novikov I.D., Thorne K.S., 1973, in: Black Holes, eds. C. DeWitt, B.S. DeWitt, Gordon and Breach, New York, p. 343
Paczyński B., Wiita P.J., 1980, A&A 88, 23
Page D., Thorne K.S., 1974, ApJ 191, 499
Phinney E.S., 1987, in: Superluminal Radio Sources, eds. J.A. Zensus, T.J. Pearson, Cambridge University Press, Cambridge, p. 301
Shakura N.I., Sunyaev R.A., 1973, A&A 24, 337
Shlosman I., Begelman M.C., Frank J., 1990, Nat 345, 679
Sikora M., Wilson D.B., 1981, MNRAS 197, 529
Szuszkiewicz E., 1990, MNRAS 244, 377
Thorne K.S., 1974, ApJ 191, 507

This article was processed by the author using Springer-Verlag TEX A&A macro package 1991.